Optimal Sizing and Control of a PV-EV-BES Charging System Including Primary Frequency Control and Component Degradation

Vermeer, Wiljan; Chandra Mouli, Gautham Ram; Bauer, Pavol

DOI
10.1109/OJIES.2022.3161091

Publication date
2022

Document Version
Final published version

Published in
IEEE Open Journal of the Industrial Electronics Society

IEEE Open Journal of the
Industrial Electronics Society

Received 19 January 2022; revised 16 February 2022; accepted 9 March 2022. Date of publication 23 March 2022;
date of current version 2 May 2022. The review of this paper was arranged by Associate Editor Marco Rivera.

Digital Object Identifier 10.1109/OJIES.2022.3161091

Optimal Sizing and Control of a PV-EV-BES Charging System Including Primary Frequency Control and Component Degradation

WILJAN VERMEER (Student Member, IEEE), GAUTHAM RAM CHANDRA MOULI (Member, IEEE), AND PAVOL BAUER (Senior Member, IEEE)

Department DC Systems, Energy Conversion and Systems, Technical University, 2628 Delft, Netherlands

CORRESPONDING AUTHOR: WILJAN VERMEER (E-mail: w.w.m.vermeer@tudelft.nl)

This work was supported by TKI urban energy.

ABSTRACT This paper proposes a method for optimally dimensioning the components of a prosumer energy management system that integrates photovoltaic (PV) panels, multiple bidirectional electric vehicle chargers, an inverter, and a battery energy storage charger. Besides optimally dimensioning the components, it also optimizes power management while integrating the frequency containment reserve market and Li-ion battery degradation. The results show that the integration of the frequency containment reserve (FCR) market can increase lifetime cost savings by 36%, compared to optimal power management alone and up to 460% compared to non-optimal power management. Furthermore, the effects of PV and battery energy storage (BES) degradation on reservable capacity are analyzed including the importance of battery second-life value on lifetime net present cost is investigated.

INDEX TERMS Battery degradation, electric vehicles, frequency control, optimal sizing, optimal power control, photovoltaic, second-life batteries.

NOMENCLATURE

PARAMETERS

ΔE_{BES}^{cal}	linearized calendar aging degradation per time step
$\Delta_{PV}(t)$	PV degradation factor per time step t [kW/t]
ϵ_{aggr}	Aggregator profit margin [0-1]
η_{BES}	Varying BES (dis)charging efficiency
η_{cable}	Power cable efficiency (EMS to meter) (0.96)
η_{ch}	Fixed (dis)charging efficiency for both BES and EV (0.98)
η_{inv}	Inverter efficiency (0.96)
η_{mppt}	Efficiency of PV maximum power point tracker (0.98)
$\lambda_{buy}(t)$	Electricity buying price at time t [€]
$\lambda_{down}(t)$	down regulation price at time t [€]
$\lambda_{sell}(t)$	Electricity selling price at time t [€]
$\lambda_{up}(t)$	up regulation price at time t [€]
$c_{1,2,3,4}(t)$	battery degradation parameter
C_{invest}	Total investment costs [€]
D_{ch}	higher limit of constant current region [−]
D_{dis}	lower limit of constant current region [−]
E_{BES}^{2nd}	Remaining battery energy storage system capacity at the start of second life [€ /kWh]
E_{EV}^{depart}	departure energy capacity
$E_X^{init/end}(i)$	Initial/final energy capacity of X = EV/BES
N_{cell}^{series}	Number of BES cell connected in series (100)
N_{series}	amount of BES cells in series
$p_{\%}$	Annual interest rate of a bank savings account [%]
$P_{appl}(t)$	appliance building load at time t [kW]
$P_{grid}^{+/-,max}$	Maximum positive/negative grid power [kW]
$P_{heat}(t)$	heating building load at time t [kW]
P_{inv}^{max}	Maximum inverter power [kW]
$P_{load}^{tot}(t)$	total building load at time t [kW]
$P_{pv,forecast}(t)$	Forecasted PV power [kW]
$P_{pv}^{irradiance}$	PV power forecast/data of a 1 kW system [kW]

P_X^{max}	Maximum (dis)charge power of X = EV/BES [kW]
$Q_{cell,nom}$	nominal BES cell capacity
T_{life}	Converter and PV system lifetime: 15 years [years]
T_{sim}	number of simulation periods in a year
V_{BES}^{2nd}	Cost per kWh for the BES (start of 2nd life) [€ /kW]
V_{BES}^{ch}	Cost per kW for the BES charger [€ /kW]
V_{BES}^{new}	Cost per kWh for the BES (new) [€ /kW]
$V_{cell,nom}$	nominal BES cell voltage
V_{EV}^{ch}	Cost per kW for the EV charger [€ /kW]
V_{inv}	Cost per kW for the inverter [€ /kW]
V_{PV}	Cost per kW for the PV system (panel+converter)[€ /kW]

INDEXES

i Amount of Electric vehicles, 1 to N

t time, $\in \{0, T\}$, where Δt is a one hour time step

VARIABLES

ΔE_{BES}	Battery capacity degradation per step t [kWh]
ΔE_{BES}^{tot}	Total lost BES capacity [kWh]
$\gamma(i,t)$	Binary parameter to set EV charging to zero outside available hours
C_{BES}	Battery Costs [€]
C_{BES}^{Ch}	Battery charger Costs [€]
C_{FCR}	Frequency Containment Reserve revenue [€]
C_{grid}	Grid Energy Costs [€]
C_{grid}	Total cost of energy
C_{int}	Interest Costs [€]
$C_{PV+conv}$	Total cost for the PV system and multi-port converter[€]
C_{total}	Total cost of energy
$D_{BES}(t)$	BES depth-of-discharge [%]
$E_{BES}(t)$	Energy content of the battery at time t [kWh]
$E_{BES}^{\%}(t)$	Percentage degradation per timestep [kWh]
$E_{BES}^{cyclic}(t)$	cyclic degradation per timestep [kWh]
$E_{BES}^{lim}(t)$	Maximum battery capacity at time t, based on degradation [kWh]
E_{BES}^{rated}	Optimized battery size at t = 0 [kWh]
$E_{EV}(i,t)$	Energy content of EV i at time t [kWh]
$I_X^{cell}(t)$	cell current of x (= BES/EV) at time t [A]
$N_{cell}^{parallel}$	Amount of battery cells in parallel [−]
$P_{BES}(t)$	Output power of battery charger at time t [kW]
$P_{BES}^{+}(t)$	Output power of battery charger at time t [kW]
$P_{BES}^{-}(t)$	Output power of battery charger at time t [kW]
$P_{BES}^{rated}(t)$	Rated power of BES charger at time t, [kW]
$P_{dwn}(t)$	Total down-regulation reserve at time t [kW]
$P_{dwn}^{X}(i,t)$	down-regulation reserve of X = EV/BES/PV at time t [kW]
$P_{EV}(i,t)$	Combined power of the ith EV at time t [kW]
$P_{EV}^{+}(i,t)$	Charging power of the ith EV at time t [kW]
$P_{EV}^{-}(i,t)$	Discharging power of the ith EV at time t [kW]
$P_{EV}^{rated}(i,t)$	Rated power of EV charger at time t, [kW]
$P_{PV}^{rated}(t)$	Maximum PV output power [kW]
$P_{FCR}^{dwn}(t)$	Combined down regulation power t [kW]
$P_{FCR}^{up}(t)$	Combined up regulation power t [kW]
$P_{grid}(t)$	Grid power at time t kW]
$P_{grid}^{+}(t)$	Positive grid power (feeding in) at time t kW]
$P_{grid}^{-}(t)$	Negative grid power at time t kW]
$P_{inv}(t)$	Inverter power at time t [kW]
$P_{inv}^{+}(t)$	Positive inverter power at time t [kW]
$P_{inv}^{-}(t)$	Negative inverter power at time t [kW]
$P_{inv}^{rated}(t)$	Rated power of EV charger at time t, [kW]
$P_{PV}(t)$	PV output power [kW]
$P_{up/dwn}^{sched}(t1:t2)$	Scheduled up/down-regulation reserve between times t1:t2[kW]
$P_{up}(t)$	Total up-regulation reserve at time t [kW]
$P_{up}^{X}(i,t)$	up-regulation reserve of X = EV/BES at time t [kW]
$P_X^{+}(i,t)$	Positive power of X = EV/BES at time t, [kW]
$P_X^{-}(i,t)$	Negative power of X = EV/BES at time t [kW]
$P_X^{max}(i,t)$	maximum charging power of X = EV/BES at time t t [kW]
$P_X^{min}(i,t)$	maximum discharging power of X = EV/BES at time t t [kW]
P_X^{rated}	Rated power of X = EV/BES at time t [kW]
$SoC_{EV}(i,t)$	State of Charge of EV i at time t [p.u.]
$SoC_X(t)$	State of Charge of X = EV/BES at time t [p.u.]
V_{BES}	Remaining value per kWh based on remaining capacity of the battery energy storage [€ /kWh]
$V_{oc}(t)$	BES open circuit voltage at time t [V]
$V_{oc}^{linear}(t)$	BES open circuit voltage at time t [V]

I. INTRODUCTION

The electrification of transportation and the built environment is an integral part of the energy transition and should be done sustainably using distributed energy resources (DERs), such as rooftop photo-voltaïc (PV) panels and energy storage systems. Smart integrated energy management systems (EMS), also known as demand response systems, are seen as smart solutions to counteract the intermittent supply and reduce the increased stress on the grid due to electrification. Recently, the emergence of aggregator services, such as [1], has given

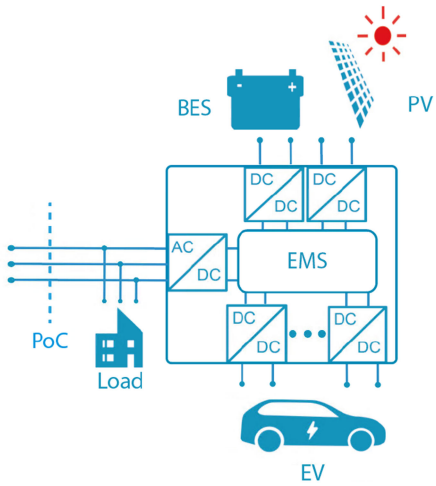

FIG. 1. Schematic of the proposed integrated energy management system (EMS).

relatively small-scale prosumers access to congestion and balancing marketplaces, such as frequency containment reserve (FCR). Besides improving grid stability, this could also reduce the relatively high return-on-investment periods for electric vehicle (EV) charging and battery energy storage (BES) systems.

This paper presents an optimization model that determines the optimal component ratings in an integrated energy management system while simultaneously optimizing its power management, including PV self-consumption, energy arbitrage, and FCR reserve capacity. The proposed EMS integrates a PV system, multiple bidirectional EV chargers, a stationary BES, and inverter, all on the same DC link. This reduces the amount of DC/AC conversion steps and total cost while increasing efficiency and power density. Here the EMS controls the EVs, BES, and PV, whereas the inverter maintains the balance on the DC link and therefore does not require an external control signal. Finally, this study assumes that a nonflexible load, consisting of a heat pump and building appliances, is connected on the AC side behind the meter. A schematic representation of this system is shown in Fig. 1.

A. RELATED WORK

The related literature is divided into two different categories 1. Studies regarding the optimal power management of integrated EMSs and 2. Studies regarding the optimal sizing of integrated EMSs. An overview of all related studies and their features is shown in Table 1. The studies are compared based on whether or not they include the following features: optimal control, optimal component sizing, optimal energy arbitrage (λ_E), optimal integration of FCR markets (λ_{FCR}), optimal EV smart charging (EV s.c.), PV self-consumption, BES or EV aging, second-life battery (SLB) value, and PV system aging.

1) OPTIMAL EMS POWER MANAGEMENT

EMSs or demand response systems are widely investigated in the literature [2], [3], [6]–[12], [44]. Among some of the common objectives is to optimize costs [3], [8], [9], [44], achieve net-zero energy [7], [10]–[12], or peak shaving [10]. Often using smart control of storages such as BES systems or EVs in combination with renewable energy resources to achieve these objectives [3]–[5], [7]–[10]. However, as seen from Table 1, many of these studies do not take into account the effects due to battery degradation, which can lead to nonoptimal results and false impressions on usable capacity, and total costs. Several studies have overcome this by a including battery degradation model. For example, to minimize operational cost of a battery swapping EV charging station [13], optimize vehicle-to-grid (V2G) charging aggregation [14], or minimizing the operational cost of an EV charging station integrated with PV and BES [15]. A different approach is used in [17] where a deep reinforced learning model is used to optimize battery energy arbitrage. Similar studies have been conducted in [16], [18].

Another effective way to reduce the total cost of energy are SLB [19], [20], which are repurposed batteries deemed unfit for their first application (generally EVs), but still have enough capacity left for other applications. In [20] a degradation model is used to assess the remaining lifetime of second-life batteries in EV charging stations. Their results show that using SLBs can reduce the total investments costs, and that degradation models are useful in prolonging battery life and maximizing their utilization.

Aside from optimized smart charging based on RES, prosumer participation in regulatory markets has recently been investigated as a way to increase revenue and overcome stability issues associated with a decentralized energy system. This is currently mainly done by utility scale BES systems or large factories. However, with the increasing amount of EVs also EV charging systems have shown to be very valuable assets for the FCR market [21], [30], [31]. Furthermore, a few studies have investigated combining the FCR market with other revenue streams. In [21] it is shown that the integration of EV smart charging, including V2G and the FCR market can save up to 317 percent on annual costs, compared to uncontrolled EV charging. Additionally, the authors of [27] show that FCR market integration can improve revenue streams by up to three times, compared to PV self-consumption alone. Similar results, on the integration and co-optimization of the FCR market and other business cases such as energy markets are obtained in [22]–[24], [26], [28].

2) OPTIMAL EMS SIZING

Because PV and BES systems are typically the most expensive components of integrated EMSs, optimizing their dimensions is critical for having a cost-effective system. [45]. In [36] the authors investigated the techno-economic feasibility of DC nano-grid by sizing the PV, EV and BES systems using a multi-objective particle swarm optimization. A similar

TABLE 1 Summary of Related Studies

Reference	Opt. control	Opt. sizing	Opt. λ_E	Opt. λ_{FCR}	EV s.c.	PV self.	BES/EV aging	SLB value	PV aging
[2]–[6]	✓		✓		✓				
[7]	✓		✓		✓	✓			
[8], [9]	✓		✓						
[6], [10]–[12]	✓					✓			
[13], [14]	✓		✓		✓		✓		
[15], [16]	✓		✓		✓	✓	✓		
[17]	✓		✓				✓		
[18]	✓		✓	✓			✓		
[19]	✓				✓	✓		✓	
[20]	✓				✓	✓	✓	✓	
[21], [22]	✓		✓	✓	✓	✓			
[23], [24]	✓		✓	✓	✓				
[22]	✓		✓	✓		✓			
[25]	✓			✓	✓		✓		
[26], [27]	✓		✓	✓					
[28]	✓		✓	✓		✓			
[29], [30]	✓		✓	✓			✓		
[31], [32]	✓			✓	✓				
[33]	✓			✓			✓		
[34]		✓		✓					
[35], [36]		✓				✓			
[37]–[39]		✓					✓	✓	
[40]–[42]	✓	✓				✓			
[43]		✓				✓		✓	
[44]		✓			✓			✓	
Proposed	✓	✓	✓	✓	✓	✓	✓	✓	✓

approach was used in [34], [35]. Some studies used battery aging models to determine BES lifetime and further optimize the BES system [36]–[38], and others have investigated the optimal size of SLBs to mitigate the intermittency of PV power in a PV-BES system [42], or for SLB assisted EV charging stations [43]. All of the above-mentioned studies use rule-based power-control schemes to determine the optimal DER dimensions. However, many studies have shown that their revenue is significantly lower then optimal power control schemes, and as a result, will lead to suboptimal results when used for sizing of optimal EMSs. Unfortunately, due to daily and seasonal variations, sizing studies require large data sets, making them unsuitable for some deterministic optimization models. This could be a potential reason why only [39]–[41] have investigated the combined optimization of power management and component sizes using, as shown in Table 1. Furthermore, Table 1 also shows that although multiple studies have been conducted to investigate the optimal control based on energy markets, FCR markets, and DER-powered EV smart charging, no study has yet addressed the optimal sizing for any of these business cases based on optimal power management.

B. CONTRIBUTION

From the literature review above, it is concluded that several studies have shown the effectiveness of EV-PV smart charging, optimal FCR market participation, or DER integration using EVs and BESs. Some studies have even looked into combining some business cases, as summarized in Table 1, and found that this can result in significantly higher gains. Next, battery degradation models have been found to be effective in prolonging lifetime and reducing the cost of ownership in both optimal control and sizing, while other studies have shown that even after batteries have degraded significantly, they still have value in second-life (SL) applications and can thus be used to reduce costs in both first- and second-life applications. Even though all these aspects have proven to reduce the total costs and help with DER integration, no study yet has integrated all of these into one optimal power management method. Furthermore, no study has yet addressed the sizing for a PV-EV-BES integrated EMS, for business cases based on optimal power management such as, smart charging, FCR market participation, PV self-consumption, or any combination of these.

Therefore, the main contributions of this paper can be summarized as follows:

1) We propose a comprehensive model for the simultaneous optimization of components ratings and their power management. Improving upon current literature, the proposed method integrates multiple business cases for smart charging such as local PV self-consumption, PV powered smart charging (including vehicle-to-grid), optimal sizing based on optimal power management, the FCR market, and second-life battery value.
2) By incorporating accurate energy storage models for both EVs and BES, and including the effects of degradation and the effect of SoC on power availability, we extend current research regarding optimal sizing and control. Due to the comprehensive model the degradation model serves multiple purposes: 1. Firstly, the degradation is minimized, and the effect of BES size on degradation is taken into account, 2. Secondly,

the actual remaining capacity is known throughout the simulation time, resulting in a more accurate trade-off between energy arbitrage and balancing reserves, 3. The BES lifetime is estimated based on its operating conditions, 4. The second-life value of the BES is assessed based on its remaining capacity, resulting in a more accurate estimation of operational and investment costs.

3) For the first time, a lifetime cost and performance analysis is performed, including the effect of component degradation on FCR market participation and total lifetime revenue. Our results indicate that EV, BES, and PV degradation and BES second-life value are significant parts of the total costs in their lifetime. To this extent, this is the first optimal sizing/control study of a new PV-EV-BES system to address the importance of second-life BES value and optimize its value during the design of the energy management system.

C. PAPER ORGANISATION

The paper is organized as follows: Section II describes the proposed Nonlinear Programming (NLP) problem. Next, the use cases will be specified in Section III. After which the obtained results are discussed in Section IV. This is followed by the Conclusion in Section V.

II. NONLINEAR PROGRAMMING MODEL

This section discusses the proposed Nonlinear Programming (NLP) model. Here C_X stands for the cost of X, V_X is the value per kW or kWh of X, P_X is the power of X, E_X is the energy of X, and λ_X is the price of X. Furthermore, superscripts $rated$ declare the optimally determined rated value of X, superscript min/max declares the time (e.g. SoC) dependent minimum or maximum of X. $+/-$ Declares a positive or negative direction, Δt stands for the timestep and i indicates a particular EV instance.

A. OBJECTIVE FUNCTION

The model's objective is to minimize the overall cost of energy to increase the attractiveness of integrated energy systems. The overall costs include the total PV and power converter costs $C_{PV+conv}$, BES degradation costs C_{BES}, grid electricity costs C_{grid}, interest costs C_{int}, and income from the primary frequency containment reserve (FCR) C_{FCR} market. A distinction for C_{BES} is made, as its performance cannot be presumed to be constant over their lifetime. The total objective function then results in:

$$min(C_{total}) = (C_{PV+conv} + C_{BES} + C_{EV} + C_{grid} + C_{int} - C_{FCR}) \quad (1)$$

1) PV - POWER CONVERTER COSTS

The optimization determines each multi-port converter component's rated power, denoted as P_X^{rated}, where X indicates the converter. In this study the converter performance is assumed to be constant over a 15 a lifetime T_{life} [46]. Therefore, the total PV and converter investment costs are denoted using (2).

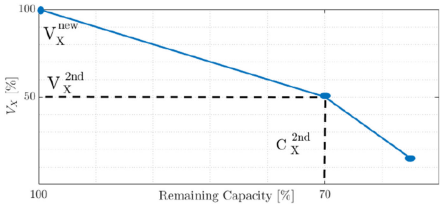

FIG. 2. Decay of value per kWh according to the model presented in [47].

Here $\frac{1}{T_{sim}T_{life}}$ is used to annualize the cost, based on a half-year simulation period. Here T_{sim} is the number of simulation periods in a year (equal to two). The PV costs per kWp V_{PV} comprise the panel cost and converter costs. Additionally, it is assumed that all values also include all possible related costs such installation costs, maintenance, development, etc, as energy outlook reports [47], [48] often combine these. The total converter investment costs are then equal to:

$$C_{PV+conv} = \frac{1}{T_{sim}T_{life}}\left(\sum_{i=1}^{n} V_{EV}^{Ch}(i)P_{EV}^{rated} + V_{BES}^{Ch}P_{BES}^{rated} + V_{inv}P_{inv}^{rated} + V_{PV}P_{PV}^{rated}\right) \quad (2)$$

2) ENERGY STORAGE DEGRADATION COSTS

The costs of battery degradation are calculated to account for the loss of capacity and loss of value, for both the BES and every ith EV. The same method is applied to all, hence the subscript $X = EV, BES$ is used for conciseness. The degradation cost C_X consider:

- The cost due to the reduction of energy capacity in kWh, calculated based on a cycle- and calendar life degradation model described in Section II.B.3.
- The cost due to the reduction of value per kWh, calculated according to the model presented in [47]. Here the remaining value per kWh is calculated based on the remaining capacity of the battery.

Based on the model presented in [47] it is assumed that the remaining value per kWh value decreases linearly with remaining capacity, the battery is in its first life, ending at 70% remaining capacity: $E_X^{2nd} = 0.7$, at 50% remaining value per kWh: $V_X^{2nd} = 50\%V_X^{new}$ [47], [49] as shown in Fig. 2 . The total degradation costs are then calculated according to (3)-(4). ΔE_{BES}^{tot} and E_{BES}^{max} indicate the total degraded capacity and maximum initial capacity, respectively, and will be calculated in section II.B.3.

$$V_X(i,t) = \frac{(V_X^{2nd} - V_X^{new})}{1 - E_X^{2nd}(i,t)}\Delta E_X^{tot}(i,t) + V_X^{new} \quad (3)$$

$$C_X = \sum_{i=1}^{n}\left((V_X^{new} - V_X(i,t))(E_X^{rated}(i,t) - \Delta E_X^{tot}(i,t))\right) \quad (4)$$

3) GRID ENERGY COSTS

Besides cost due to degradation, another part of the operational expenditure are the grid electricity costs. A distinction between $P^{+}_{grid}(t)$ and $P^{-}_{grid}(t)$ is made in order to account for the difference in price. The resulting cost are given in (5).

$$C_{grid} = \sum_{t}^{T} P^{+}_{grid}(t)\Delta t \lambda_{buy} - \sum_{t}^{T} P^{-}_{grid}(t)\Delta t \lambda_{sell} \quad \forall t \tag{5}$$

4) INTEREST COST

The cost of interest is equal to the potential income received if no expenditure had been made. Here the EVs are not taken into account, as they are assumed to be bought independently from the proposed EMS. An annual interest $p_{\%}$ of 1% is taken into account, the resulting interest cost is then calculated according to (6)-(7). If the simulation period covers multiple years, (7) can be multiplied with an amortization rate A as shown in (8)

$$C_{invest} = V^{new}_{BES} E^{rated}_{BES} + C_{PV+conv} \tag{6}$$

$$C_{int}(t) = C_{invest}\, p_{\%} \frac{1}{T_{sim}} \qquad \forall t \tag{7}$$

$$A = \frac{p_{\%}(p_{\%}+1)^{n}}{(p_{\%}+1)^{n}-1} \tag{8}$$

5) FREQUENCY CONTAINMENT RESERVE

The last part of the objective function is the revenue obtained from the primary frequency containment reserve (FCR) market. Based on a pilot study regarding prosumer FCR market participation in the Netherlands [50], it is assumed that a third party acts as an aggregator, combining several systems to reach the minimum bidding power requirement for FCR market participation. Revenue is then generated by reserving a part of the available power capacity for up/down-regulation [51], here denoted as P^{up}_{reg} and P^{dwn}_{reg}, respectively. The up/down-regulation prices are: $\lambda_{up}, \lambda_{dn}$ (obtained from [52]), respectively, and ϵ_{agg} is a margin between 0 and 1, used to denote the cost of aggregation. Based on regulation prices, the operational costs, and the current demand, the optimization will determine how much of the available power capacity to reserve for regulation. Calculated in the constraints below. The total obtained revenue is then equal to:

$$C_{FCR} = (1-\epsilon_{agg}) \times \eta_{inv}\eta_{ch} \sum_{t=1}^{T} \Big(P_{up}(t)\lambda_{up}(t) + P_{dwn}(t)\lambda_{dwn}(t) \Big) \forall t \tag{9}$$

Note that only the revenue obtained from acting as reserve is taken into account as the net energy delivered is assumed zero. This concludes the objective part of the model. The next section discusses the model constraints.

B. CONSTRAINTS

1) POWER BALANCE & LIMITATIONS

Fig. 1 shows a schematic representation of the proposed system. In this study, positive BES/EV power denotes charging operation, and positive grid power is equal to feeding power to the grid. For the given system, two power balances exist: 1. The first power balance is on the DC link of the multi-port converter:

$$P_{inv}(t) = P_{PV}(t) - P_{BES}(t) - P_{EV}(t) \quad \forall t \tag{10}$$

(11)-(12) model the maximum power point tracking of the PV converter. The model becomes more flexible by allowing PV power curtailment during negative electricity prices or oversized PV systems. Here the symbol η_{mppt} is used to model converter efficiency, which equals 98%[53]. $\Delta_{PV}(t)$ represents the degradation of the PV panels, which is included as a linear decay of 1% a year [54].

$$P_{PV}(t) \leq \eta_{mppt}(1-\Delta_{PV}(t))P^{irradiance}_{PV}(t)P^{rated}_{PV} \quad \forall t \tag{11}$$

$$P_{PV}(t) \geq 0 \qquad \forall t \tag{12}$$

Next, for all bidirectional converters, a distinction is made between positive and negative powers to account for the converter's efficiency. This is described using (13)-(15). Here η_{BES}, η_{EV}, and η_{inv} are equal to 97.5% (initially), 97.5%, and 97% for the BES charger, EV charger, and inverter, respectively. For the EV and BES it also includes the battery losses of a single charging or discharging instance [55]. Furthermore, the BES and EV's internal resistance increases due to degradation. This is accounted for by making it dependent on $E^{lim}_{X}(t)$, according to 15). It is assumed that the internal resistance is doubled, when the battery reaches 70% of its nominal capacity [56], [57].

$$P_{X}(i,t) = \eta_{X} P^{+}_{X}(i,t) - \frac{1}{\eta_{X}} P^{-}_{X}(i,t) \qquad \forall t \tag{13}$$

$$P_{inv}(i,t) = \eta_{inv} P^{+}_{inv}(i,t) - \frac{1}{\eta_{inv}} P^{-}_{inv}(i,t) \qquad \forall t \tag{14}$$

where,

$$\eta_{X}(i,t) = \eta_{ch} - 0.025 \frac{E^{rated}_{X}(i) - E^{lim}_{X}(i,t)}{0.3 * E^{rated}_{X}(i)} \quad \forall t \tag{15}$$

with X equal to EV or BES. Besides being limited by the converter's rated power, the EV and BES are also limited by the maximum amount of power that can be drawn from their batteries. This is dependent on the size of the battery combined with its maximum C-rate. For stationary applications, this is often limited to 1 C (or lower) [55]. Apart from ultra-fast charging applications, EV charging is usually below 1 C as well. Therefore, a maximum C-rate of 2 is considered and modeled using (16). Additionally, the maximum charging powers P^{max}_{X} and maximum discharging power P^{min}_{X} are dependent on the State-of-charge (SoC) of the battery. This dependency divides the (dis)charging regions into the regions known as precharge region (very low SoC), constant-current (CC) region, and constant-voltage (CV) region. Because the

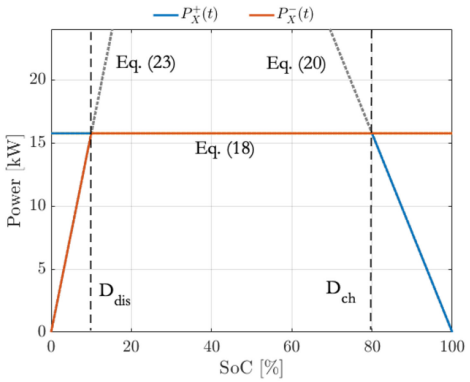

FIG. 3. Graphical representation of $P_X^+(t)$ and $P_X^-(t)$, where $D_{dis} = 0.1$, $D_{ch} = 0.8$, and $P_X^{rated} = 15.75$.

maximum C-rate is 2 C, the maximum power in the CC-region is restricted by the converter's operational power limit P_X^{OP} a constant power. A graphical representation of the three charging regions, and the corresponding power limit is shown in Figure 3. These power limitations are often neglected charging studies, but impacts the available power. The charging regions are modelled using (17)-(22). Here $D_{ch/dis}$ denote the upper and lower SoC limit of the CC-region.

$$P_X^{rated} \leq 2E_X^{rated} \tag{16}$$

$$P_X^+(i,t) \leq P_X^{max}(i,t) \quad \forall t \tag{17}$$

$$P_X^{max}(i,t) \leq P_X^{op}(i) \quad \forall t \tag{18}$$

$$P_X^{max}(i,t) \leq \frac{P_X^{op}}{(1-D_{ch})}\left(\frac{E_X(i,t)}{E_X^{rated}} - 1\right) \quad \forall t \tag{19}$$

$$P_X^-(i,t) \leq P_X^{min}(i,t) \quad \forall t \tag{20}$$

$$P_X^{min}(i,t) \leq P_X^{op}(i) \quad \forall t \tag{21}$$

$$P_X^{min}(i,t) \leq \frac{P_X^{op}(i,)}{D_{dis}}\frac{E_X(t)}{E_X^{rated}} \quad \forall t \tag{22}$$

Here P_X^{op} is used to divide the rated power of P_X^{rated} into an operational part P_X^{op}, and a reserve capacity (FCR) part P_X^{FCR}. P_X^{op} is then the power available for the operational scheduling of X, where is P_X^{FCR} is reserved for FCR capacity. This ensures that there is always enough power available for FCR provision and SoC-management. During FCR provision, both regions are available depending on the frequency deviation. The distinction is made according to (23).

$$P_X^{rated}(i) = P_X^{op}(i) + P_X^{FCR}(i) \tag{23}$$

The second power balance in the system is on the AC side between the inverter and the meter. Here the appliance load $P_{load}(t)$ and heating load P_{heat} are connected, as modelled using (24).

$$P_{grid}(t) = P_{inv}(t) - P_{appl.}(t) - P_{heat}(t) \quad \forall t \tag{24}$$

In this case, both the appliance load and heating load are considered inflexible and therefore do not require any additional constraints. Using (25)-(27) the grid power is constrained by $P_{grid}^{+/-,max}$, which can be allocated dynamically allowing for power curtailment.

$$P_{grid}^-(t) \leq P_{grid}^{-,max}(t) \quad \forall t \tag{25}$$

$$P_{grid}^+(t) \leq P_{grid}^{+,max}(t) \quad \forall t \tag{26}$$

$$P_{grid}(t) = \eta_{cable}P_{grid}^+(t) - \frac{1}{\eta_{cable}}P_{grid}^-(t) \quad \forall t \tag{27}$$

Due to the difference between retail electricity price and feed-in tariff (FIT), it is important to distinguish between positive and negative grid power. Often this is done using binary variables [21], [58]. However, the use of binary variables, especially in combination with nonlinear constraints, drastically increases the solving time of any deterministic optimization problem. In order to solve this problem the efficiency η_{cable} is introduced as a soft constraint to let the optimization recognizes the efficiency loss and prevents simultaneous nonzero values for $P_{grid}^+(t)$ and $P_{grid}^-(t)$. This is valid on the condition that the FIT is always below the retail price. However, in any practical scenario, this will be true.

2) ENERGY BALANCE & LIMITATIONS

The degradation model used in this study is developed for a single Li-ion cell. Therefore it is assumed that $N_{cell}^{parallel}$ by N_{cell}^{series} of these cells make up the total battery pack of the BES. The energy capacity of the battery pack is then determined by the variable $N_{cell}^{parallel}$, and $N_{cell}^{series} = 100$ cells are used to produce the required battery voltage, as modeled by (28). The equation is divided by a thousand in order to obtain a kWh unit. Here V_{cell}^{nom} and Q_{cell}^{nom} are the nominal open-circuit voltage and charge of a single 18650 NMC cell, in this case 3.7 V and 1.5Ah, respectively.

$$E_{BES}^{rated} = \frac{N_{cell}^{series}N_{cell}^{parallel}}{1000}V_{cell}^{nom}Q_{cell,nom} \tag{28}$$

(28) describes the initial maximum energy capacity. However, over time this maximum capacity will decrease by $\Delta E_{BES}(t)$, which is determined by the battery degradation model discussed in Section II.B.3. Updating the maximum available capacity is modelled using (29)-(30).

$$E_{BES}^{lim}(t) = \begin{cases} E_{BES}^{rated}, & \text{for } t = 1 \\ E_{BES}^{lim}(t-1) - \Delta E_{BES}(t), & \text{for } t > 1 \end{cases} \tag{29}$$

$$E_{BES}(t) \leq E_{BES}^{lim}(t) \quad \forall t \tag{30}$$

Next, to calculate the degradation and power limitations, the SoC needs to be calculated based on the newly found maximum capacity, for the EVs $E_X^{lim} = E_{EV}^{max}$. This is done using (31). It is assumed that the all SoC_X are allowed to range from 10-100%, see (32). Furthermore, (33) is used to equate the beginning and endpoint SoC to have a fair comparison of

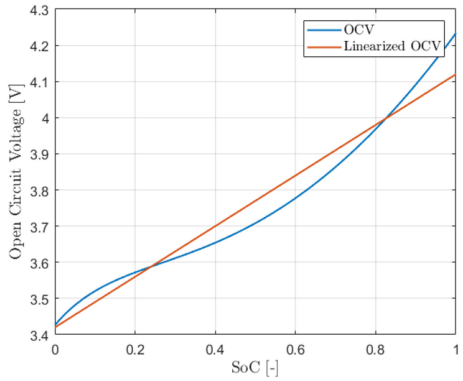

FIG. 4. Open circuit voltage for a NMC battery cell [60] and its linearized variant.

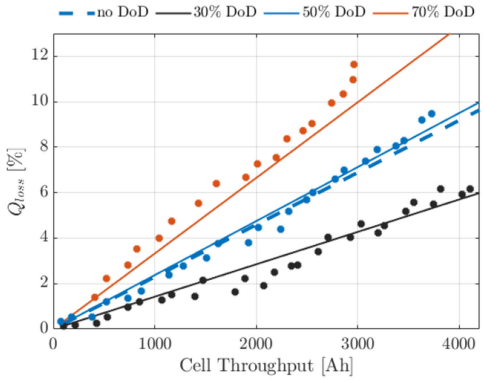

FIG. 5. The dots indicate the results of the cell aging tests presented in [59]. The cells are tested at a C-rate of 3.5 C, T = 34 °C and with a DoD equal to 30, 50 and 70%.

energy costs. Again the subscript X is used to denote the BES, or any ith EV.

$$SoC_X(i,t) = \frac{E_X(i,t)}{E_X^{lim}(i,t)} \qquad \forall t \tag{31}$$

$$0.1 \leq SoC_X(i,t) \leq 1 \qquad \forall t \tag{32}$$

$$E_X(i,t) = \begin{cases} E_X^{init}(i), & \text{for} \quad t = 1 \\ E_X^{end}(i), & \text{for} \quad t = T \end{cases} \tag{33}$$

Finally, the amount of energy inside the BES and EV at each timestep is calculated according to (34) and (35), respectively.

$$E_{BES}(t) = E_{BES}(t-1) + P_{BES}(t)\Delta t \qquad \text{for} \quad t > 1 \tag{34}$$

$$E_{EV}(i,t) = E_{EV}(i,t-1) + (\gamma(i,t)P_{EV}(i,t) - P_{drive}(i,t))\Delta t \qquad \text{for} \quad t > 1 \tag{35}$$

in (35) parameter $\gamma(i,t)$ is used to set $P_{EV}(t)$ to zero when the EV is not available and $P_{drive}(i,t)$ is used to model the reduction of energy due to driving when the EV is not available. Additionally, $P_{drive}(i,t)$ helps by ensuring that (35) is valid over the entire simulation period, therefore preventing the use for conditional statements in case the EV is unavailable. Finally, a minimum departure charge can be set by the user using (36).

$$E_{EV}(i,t) = E_{EV}^{depart} \qquad for\, t > t_{depart} \tag{36}$$

3) ENERGY STORAGE DEGRADATION MODEL

The remaining capacity of the BES and every ith EV is required to determine the cost of degradation and to accurately optimize power management. The used model is based on the one presented in [59]. However, a depth of discharge dependency is added based on data presented in the same study. Fig. 5 shows the improved accuracy. The model is based on a single NMC cell; therefore, the power $P_X(i,t)$ is translated into the voltages and currents of a single cell using (37)-(38), assuming perfect cell balancing. In order to reduce the solving time, (37) is the linearized form of the open-circuit voltage of an NMC cell [60], as shown in Fig. 4. Next, the cyclic and calendar aging are calculated according to (40)-(42). Here a calendar degradation rate of 2% per year at 20 °C is assumed [61]. This is linearized to a fixed percentage per time step c_6. For every EV, the degradation due to driving is calculated based on the WLTC profile, assuming 2 trips of 23 km on every weekday. The resulting degradation is averaged per time step and added to c_6. Since the power rating of the EV and BES chargers is limited to 1 C, which is far below the maximum C-rate of the cells, the power handling capability of the BES/EV will not be affected in its lifetime. However, to account for the increase in internal resistance, the efficiency is modelled as a function of remaining capacity, using (15). Here it is assumed that the internal resistance is doubled when it reaches 70% remaining capacity [56][57].

$$V_{oc}^{linear}(i,t) = N_{cell}^{series}(i)(3.42 + 0.7SoC_X(i,t)) \quad \forall i,t \tag{37}$$

$$i_X^{cell}(i,t) = \frac{P_X(i,t)}{N_{cell}^{parallel}(i)V_{oc}^{linear}(i,t)} \qquad \forall i,t \tag{38}$$

$$\Delta E_X^{\%}(i,t) = c_1 e^{c_2|I_X^{cell}(i,t)|}\frac{c_3 D_X(i,t)}{c_4}|I_X^{cell}(i,t)|\Delta t \qquad \forall i,t \tag{39}$$

$$\Delta E_X^{cycle}(i,t) = (\Delta E_X^{\%}(i,t))\frac{E_X^{rated}(i)}{100} \quad , \forall i,t \tag{40}$$

$$\Delta E_X^{cal}(i,t) = \left(c_5\sqrt{t}e^{-24\,kJ/RT}\right)\frac{E_X^{rated}(i)}{100} = (c_6\Delta t)\frac{E_X^{rated}(i)}{100} \qquad \forall i,t \tag{41}$$

$$\Delta E_X^{tot}(i) = \sum_{t=0}^{T}\left(\Delta E_X^{cycle}(i,t) + \Delta E_X^{cal}(i,t)\right) \quad \forall i,t \tag{42}$$

4) FREQUENCY CONTAINMENT RESERVE CONSTRAINTS

Finally, the primary frequency containment reserve (FCR) constraints. The available reserve capacity is determined as the difference between the components' maximum positive, negative or rated power (P_X^{max}, P_X^{min}, and P_X^{rated}) and the

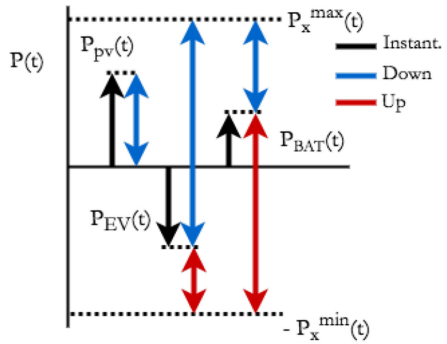

FIG. 6. Concept of available reserve capacity shown per component (EV, PV, BES). The black arrows indicate the instantaneous powers, whereas the blue and red arrows represent the down- and up-regulation, respectively.

current/scheduled power $P_X(t)$. Taking into account power ratings, SoC limitations, both AC and DC power balances in the system, and the total appliance and heating load. This concept per component is shown in Fig. 6 and is calculated analogously for up- and down regulation using (43)-(50) and (51)-(59), respectively.

$$P_{up}^{EV}(t) \leq \gamma(i,t) \sum_{i=1}^{n} \left(P_{EV}^{FCR}(i) \right) \forall\, t \tag{43}$$

$$P_{up}^{EV}(t) \leq \gamma(i,t) \sum_{i=1}^{n} \left(\frac{E_{EV}^{rated}(i) - E_{EV}(i,t)}{\Delta t} \right) \tag{44}$$

$$P_{up}^{BES}(t) \leq P_{BES}^{FCR} \qquad \forall\, t \tag{45}$$

$$P_{up}^{BES}(i,t) \leq \frac{E_{BES}(i,t) - E_{BES}^{rated}}{\Delta t} \tag{46}$$

$$P_{up}^{BES}(t) \geq 0, \quad P_{up}^{EV}(t) \geq 0, \quad P_{up}(t) \geq 0 \quad \forall t \tag{47}$$

$$P_{up}(t) \leq \eta_{inv} \left(P_{up}^{EV}(t) + P_{up}^{BES}(t) \right) \qquad \forall\, t \tag{48}$$

$$P_{up}(t) \leq P_{inv}^{rated}(t) - P_{inv}(t) \qquad \forall\, t \tag{49}$$

$$P_{up}(t) \leq P_{grid}^{max}(t) - P_{inv}(t) + P_{appl}(t) + P_{heat}(t) \forall\, t \tag{50}$$

$$P_{dwn}^{EV}(t) \leq \gamma(i,t) \sum_{i=1}^{n} \left(P_{EV}^{FCR}(i) \right) \qquad \forall\, t \tag{51}$$

$$P_{dwn}^{EV}(t) \leq \gamma(i,t) \sum_{i=1}^{n} \left(\frac{E_{EV}(i,t) - E_{EV}^{min}(i,t)}{\Delta t} \right) \tag{52}$$

$$P_{dwn}^{BES}(t) \leq P_{BES}^{FCR} \qquad \forall\, t \tag{53}$$

$$P_{dwn}^{BES}(t) \leq \frac{E_{BES}(t) - E_{BES}^{min}(t)}{\Delta t} \tag{54}$$

$$P_{dwn}^{PV}(t) \leq P_{PV}(t) \qquad \forall\, t \tag{55}$$

$$P_{dwn}^{PV}(t) \geq 0, \; P_{dwn}^{BES}(t) \geq 0, \; P_{dwn}^{EV}(t) \geq 0, \; P_{dwn}(t) \geq 0 \; \forall t \tag{56}$$

TABLE 2 EV demand [63][64]

Quantity	Value
availability weekday	08:00h-18:00h
availability weekend	-
number of EVs	3
energy demand weekday (EV1, EV2, EV3)	15,30,5kWh

$$P_{dwn}(t) \leq \eta_{inv} \left(P_{dwn}^{EV}(t) + P_{dwn}^{BES}(t) + P_{dwn}^{PV}(t) \right) \forall\, t \tag{57}$$

$$P_{dwn}(t) \leq P_{inv}^{rated}(t) + P_{inv}(t) \qquad \forall\, t \tag{58}$$

$$P_{dwn}(t) \leq P_{grid}^{max}(t) + P_{inv}(t) - P_{appl}(t) - P_{heat}(t) \forall\, t \tag{59}$$

In some countries FCR should be contracted symmetrically, in those cases (60) should be included. Finally, in order for the model to work in a moving horizon context, (61) and (62) are added to ensure that the power reserved in the day-ahead is actually available. Here $t + t_1 : t + t_2$ indicates the time frame in which the powers are reserved.

$$P_{up}(t) = P_{dwn}(t) \tag{60}$$

$$P_{FCR}^{up}(t + t_1 : t + t_2) = P_{FCR,sched}^{up}(t1 : t2) \tag{61}$$

$$P_{FCR}^{dwn}(t + t_1 : t + t_2) = P_{FCR,sched}^{dwn}(t1 : t2) \tag{62}$$

.

III. CASE STUDIES

The effectiveness of the proposed methodology is demonstrated using an office building with three EV chargers. Due to its fixed working hours and multiple EV charging spots, an office building is well suited for integrating regulatory services. The results will be compared using three use cases.

- **case 1:** The proposed model, assuming asymmetrical reserves.
- **case 2:** The proposed model, assuming symmetrical reserves.
- **case 3:** The proposed model, without FCR constraints (43)–(59).
- **case 4:** A particle swarm optimization (PSO) based component size optimization, combined with a rule-based power control algorithm based on the algorithm described in [36].

The simulations are run for a half year, based on data from January to June 2018, to capture all diurnal and seasonal variations. Here, we assume that the seasonal fluctuations in the first half of the year are similar to those in the second half of the year to reduce the solving time. Further examination shows that this does not affect the component sizes and therefore is a reasonable assumption. The electrical and heating demand profiles ($P_{load}(t)$ and $P_{heat}(t)$, respectively) are considered non-flexible and are obtained from [62], see Fig. 7 for two exemplary days. The EV charging patterns are obtained from [63], [64] and are summarized in Table 2 . The PV irradiance data is obtained from the Dutch Meteorology Institute [65].

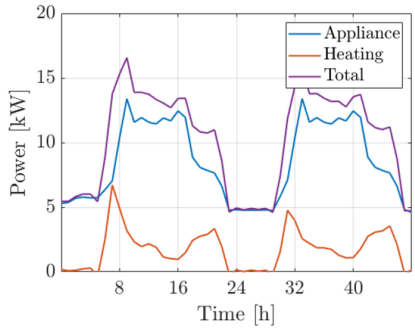

FIG. 7. Two exemplary days of the appliance and heating load ($P_{appl}(t)$, $P_{heat}(t)$) obtained from [62].

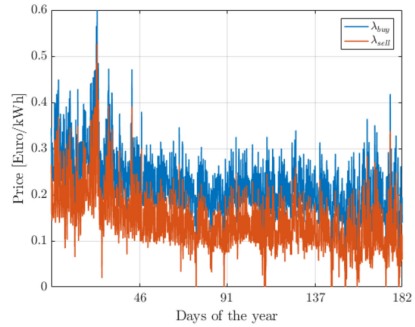

FIG. 8. Energy prices λ_{buy}, λ_{sell}, based on the 2018 APX market but averaged around 20 cents/kWh for agreement with consumer electricity prices.

The electricity prices (λ_{buy}, λ_{sell}) are based on the Amsterdam Power Exchange (APX) day-ahead market, though yearly averaged around 20 cents/kWh to be comparable with current retail electricity prices. For the same reason, FIT is chosen at 50% of the average retail price tariffs [36], see Fig. 8. Finally, the regulation prices are obtained from the Dutch frequency regulation market [52].

IV. RESULTS

In this section, the results will be discussed based on the three use cases described above. Besides the optimal power management, the optimization will determine the:

- Battery energy capacity E_{bat}^{max} [kWh]
- Battery charger power rating P_{bat}^{max} [kW]
- PV system power rating P_{PV}^{max} [kW]
- EV charger power rating P_{EV}^{max} [kW]
- Inverter power rating P_{inv}^{max}[kW]

The variable bounds are given in Table 2. The model has been solved with the CONOPT4 solver on the Generic Algebraic Modeling System (GAMS) on a desktop computer with a 3.6 GHz Intel Xeon 4 core and 16 GB RAM.

A. OPTIMAL POWER MANAGEMENT & COMPONENT SIZE

The power flows for the four cases are shown in Figs. 9(a)–(d), the optimal component sizes are given Table 3, and the optimal cost components are given in Table 4. The ratio's of operational capacity (P_X^{op}) to rated capacity (P_X^{rated}) for the

TABLE 3 Sizing Variable Prices and Bounds

Type	Bounds	Price
PV system	0-50kWp	1500 €/kWp [67]
Battery system	0-200kWh	500 €/kWh [49]
BES charger	0-200kW	300 €/kW [68]
EV charger	0-200kW	350 €/kW [68]
Inverter	0-200kW	300 €/kW [47]

TABLE 4 Cost Component for Each Use Case

Variable	case 1	case 2	case 3	case 4
C_{grid}	€2280	€3233	€2808	€4131
C_{BES}	€1224	€1545	€334	€0
C_{EV}	€975	€972	€1060	€1037
$C_{PV+conv}$	€4620	€4065	€3218	€3060
C_{FCR}	€-4337	€-4710	€0	€0
C_{int}	€1002	€997.5	€567	€461
C_{total}	€5764	€6102.5	€7987	€8689

BES and EV1-3 equal are also given in Table 3. The PV size is equal to the maximum 50 kWp for all cases. This can be explained by PV's Levelized Cost of Energy (LCOE) as calculated according to (63). Since the LCOE is lower than the FIT for 82% of the time, the PV system is a profitable investment and the optimization maximizes it size.

$$LCOE = \frac{V_{PV} P_{PV}^{max}}{\sum_{t=0}^{T} (P_{PV}\,\Delta t) T_{life} T_{sim}} = 0.0931€/kWh \quad (63)$$

Notice that the PV-inverter power ratio is greater than one for cases 3 and 4. This is a result of the often low irradiance of the Dutch environment. By having a smaller inverter it better utilizes its entire power range. Another reason is that the EV, BES, and PV are all connected on the inverter's DC side and can therefore absorb part of its power. Contrary to the PV system, the BES is not a profitable investment for case 4. This is a result of the fact that there is already a good simultaneity between supply (PV) and demand (load, heating & EV). In combination with the fact that the BES is operated based on the net power in the system. Consequently, the BES is seldom used in winter; when heating demand is higher and solar irradiance is lower. This is different for cases 1-3, as the control anticipates on future supply and demand, it optimizes the BES's (dis)charging to take advantage of differences in electricity price. Similarly, the charging of the EVs is also optimized, and vehicle-to-grid (V2G) is used to minimize operational costs. As a result, the cost of grid energy for cases 1-3 is 44.8%, 21.7% and 32% lower compared to in case 4, respectively. The benefit of optimal power management is even higher for use cases with lower supply-demand simultaneity and/or lower PV output, such as residential buildings. Table 3 also shows the effect of the FCR market constraints; the power- and energy ratings of cases 1 and 2 are significantly higher than case 3, especially for case 1. Obviously, higher component ratings result in more reserve power available to be exchanged on the FCR market and more energy available to be arbitrated. Due to this increased revenue, the total costs were reduced by 27.8% and 23.6%, compared to case 3. The difference in power ratings demonstrates the importance of

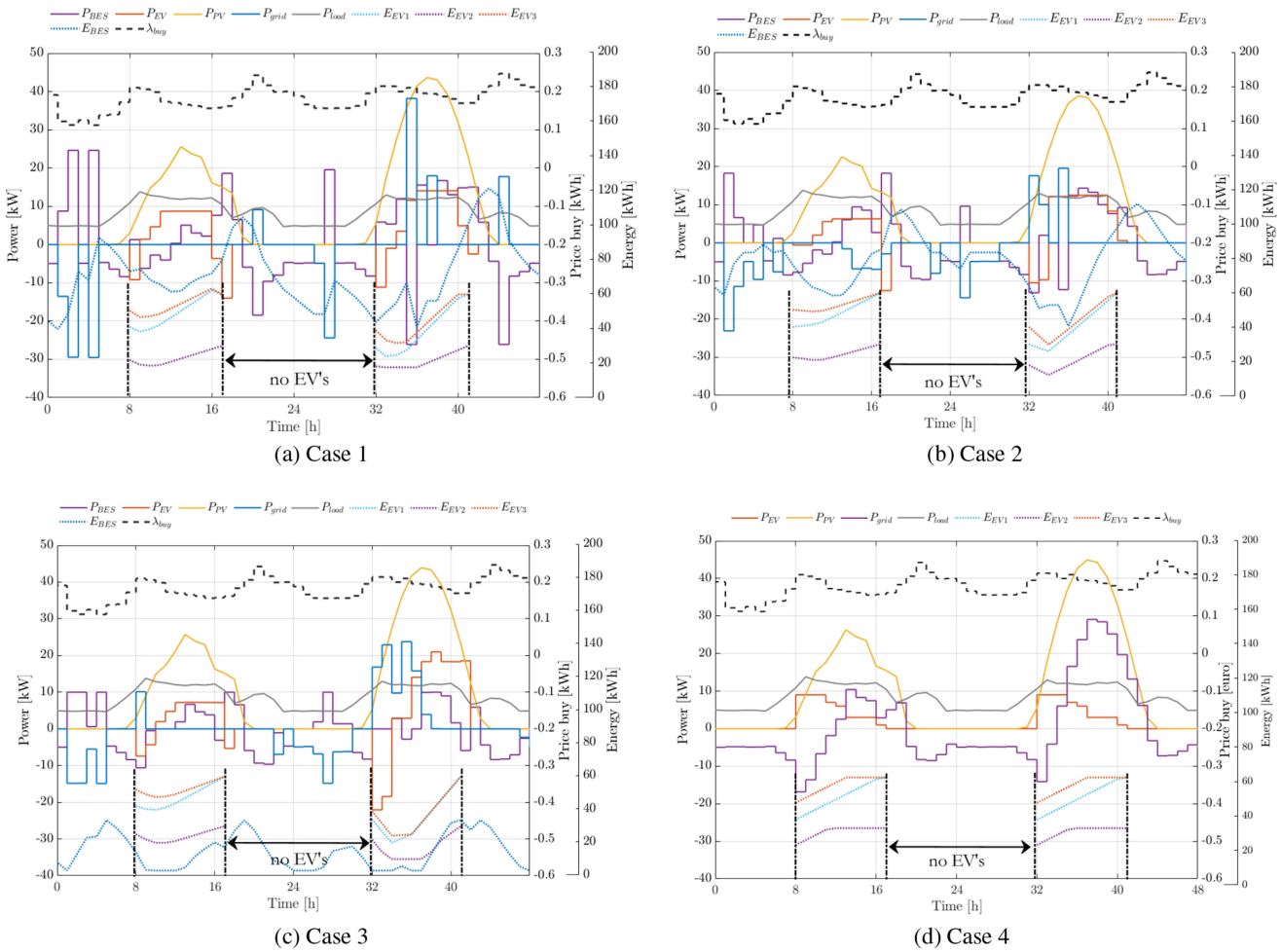

FIG. 9. **Power and energy (dotted lines) flows for all four cases. The grid energy price is also plotted in striped lines for reference.**

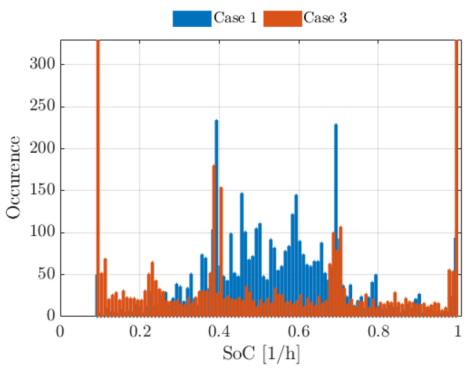

FIG. 10. **Occurence of BES SoC [%] for cases 1 and 3. The case 1 BES operates mostly in the 30-80% region, to ensure that it always has reserve capacity available for FCR market participation.**

TABLE 5 **Optimal Component Sizes for Each Use Case**

Variable	case 1	case 2	case 3	case 4
P_{PV}^{max}	50 kWp	44 kWp	50 kWp	50 kWp
E_{BES}^{max}	123.6 kWh	156 kWh	33.7 kWh	0 kWh
P_{BES}^{rated}	100 kW	91 kW	10 kW	0 kW
P_{BES}^{Op}	25 kW	18.8 kW	10. kW	0 kW
P_{EV}^{rated}	10 kW	5 kW	7.2 kW	2.8 kW
P_{EV1}^{Op}	6 kW	5 kW	7.2 kW	0 kW
P_{EV2}^{Op}	2.5 kW	3 kW	7.2 kW	0 kW
P_{Ev3}^{Op}	5.7 kW	5 kW	7.2 kW	0 kW
P_{inv}^{max}	77 kW	78 kW	36.6 kW	46 kW

including the FCR constraints when optimizing component sizes. Note that optimal power management at the same time further lowers costs, as it calculates the optimum trade-off between operating capacity, reserve capacity, and degradation. The BES SoC profiles in Fig. 9(a)–(b) and the SoC histograms in Fig. 10 are an example of this. These show that the case 1 BES is seldom completely charged or discharged, but remains mostly in the 30-80% SoC area. As a consequence, the BES always has up/down-regulation power available. Whereas the BES in case 3 generally uses its entire allowable SoC range. Based on the results presented so far it is concluded that FCR market participation can significantly increase the scheduled revenue. However, so far the effects of FCR provision, in terms of grid electricity costs and degradation, have not been taken into account. These additional costs are analyzed using a moving horizon control scheme in the next section.

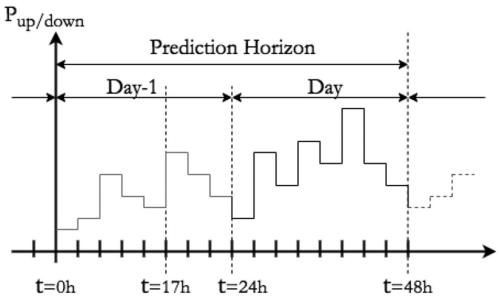

FIG. 11. Moving horizon control window, with a prediction horizon equal to 48 h. The FCR is procured every day at 17:00 h the day ahead.

TABLE 6 Summary of Results for Cases 1-4. The Percentage Cost Savings are Calculated by Comparing Them With Case 4

	case 1	case 2	case 3	case 4
Cost savings[%]	460%	395%	337%	0
ROI [years]	11.7	12.3	10.2	12.5
Lifetime BES [years]	13.5	14.5	13.8	n.a.
Lifetime EV1 [years]	10.6	10.7	10.2	11.9
Lifetime EV2 [years]	8.2	8.6	8.6	9.5
Lifetime EV3 [years]	10.6	10.7	10.2	11.9

B. LIFETIME NET PRESENT COSTS

To consider the additional costs due to FCR provision and PV forecast uncertainty, the total lifetime Net Present Costs C_{NPC} and Return On Investment (ROI) periods are calculated using the proposed model in a moving horizon context as shown in Fig. 13. Here, the rules from a pilot study on prosumer FCR market participation in the Netherlands [50] are adopted. Here asymmetrical aggregation and assuming day-ahead procurement (as shown in Fig. 11) are used.The FCR power is bid hourly but provided in a one-minute resolution. A linear SoC-management technique ensures that the energy storages at $t = t + 1$ equal the scheduled capacities. Furthermore, 1-minute resolution PV data accounts for the PV forecasting errors. Consequently, the resulting power flows are all in a 1-minute resolution. In this analysis, the EV degradation is minimized, but the related costs are not factored in as the EVs are privately owned.

This moving horizon is simulated for a 15 a period. After which, C_{NPC} is calculated using (64).

$$C_{NPC} = C_{invest} - (C_{base} - C_{total}) \tag{64}$$

Here C_{base} is the demand only expense (appliance, heating and EV), and thus $(C_{base} - C_{total})$ are the energy management system's savings. Fig. 12(a) shows that the ROI period equals 11.7 years, 12.3 years, 10.2 years, and 12.5 years for cases 1-4, respectively. Therefore all cases are profitable investments, achieving total lifetime profits of € 22.7 k, € -7.5 k € 42.7 k, € 17.4 k, respectively. However, after including the remaining second-life values of the BESs, as calculated according to (3)(4), the profits of cases 1-3 increase further to € 80 k, € 68.8 k, € 58.7 k, respectively. The total savings, ROI, and lifetimes of cases 1-3 are summarized in Table 6. Different to the results obtained in Table 4 these results include the additional costs (or reduction in revenue) due to component degradation, PV forecasting errors, and FCR power provision. An example of the difference between optimal scheduled grid power and actual grid power is shown in Fig. 12(b), which shows that power provided for FCR significantly deviates the grid power from its optimal schedule. As a result, the total grid energy cost increases by 29.4% and 22.2% for cases 1 and 2, respectively. As shown in Fig. 12(c). This difference in grid power is provided by the BES and EVs, and this additional cycling can also increase the degradation of their batteries. As summarized in Fig. 12(c), the BES degradation has increased by 2-4.5%, compared to the same case without FCR provision. Since the mean frequency deviation is close to zero, the additional degradation of the battery is less significant than the increase in grid energy costs. Nonetheless, despite these increased costs, it can be concluded that the FCR market can be effectively integrated with other revenue streams such as energy arbitrage and PV self-consumption and is an effective method for lowering overall costs. Furthermore, our results show that BES and EV 2nd-life value is a significant part of the overall lifetime profit. The effect of component degradation and 2nd-life value is discussed in more detail in the next section.

C. EFFECT OF COMPONENT DEGRADATION

The degradation of the EV, BES, and PV systems are calculated over the entire moving horizon period (15 years), and once these reach their end-of-life criteria of 70% remaining capacity, they are replaced and sold for their second-life value. This is observed in Fig. 12(a) as the stepwise increase in cost. The resulting lifetimes of the EVs and BES are summarized in Table 6. The reduced degradation of case 2 with respect to case 1 can be explained by the fact that the case 2 BES operates at a lower C-rate, as shown in Fig. 14. Additionally, the normalized throughput per cell of the case 2 BES is almost 52% lower compared to case 1. This is because the model tries to maximize the FCR revenue, and due to the symmetrical bidding constraint, has less capacity available for other revenue streams such as energy arbitrage. Finally, please note that for both cases, the C-rates are much lower than the maximum allowable 2 C, due to the BES degradation model.

To analyze the effectiveness of the degradation model, the case 1 model has been run without BES degradation model assuming a fixed 15 a lifetime over which the costs are annualized. The optimal BES size now became 97 kWh with a rated power of 113, and since the 2nd-life value was not considered C_{BES} increased by 32%. When the degradation of the resulting BES profile was calculated, it was 17% higher than the case 1 BES, which would result in a 2 a and 4 mo reduction of lifetime. Another important feature of the degradation model is calculating the available energy capacity. To examine the effect of component degradation on revenue, we examine the differences in revenue for case 1 in the first half year versus the first half of year 13, just before BES replacement. The resulting difference in grid energy costs and FCR revenue are

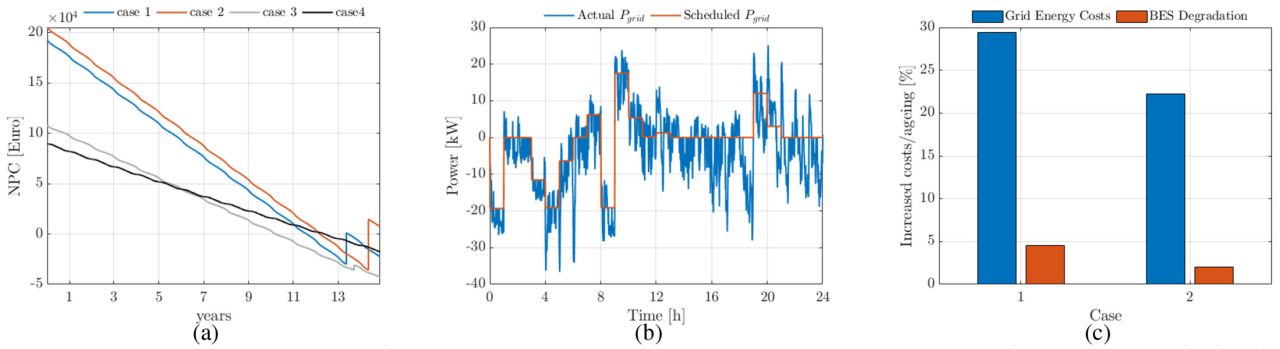

FIG. 12. **(a):Net Present Cost of the four analyzed cases (excluding second-life BES values). (b): Actual vs. Scheduled grid power, as a result of FCR power provision. (c): Increased cost (energy and degradation) due to FCR power provision.**

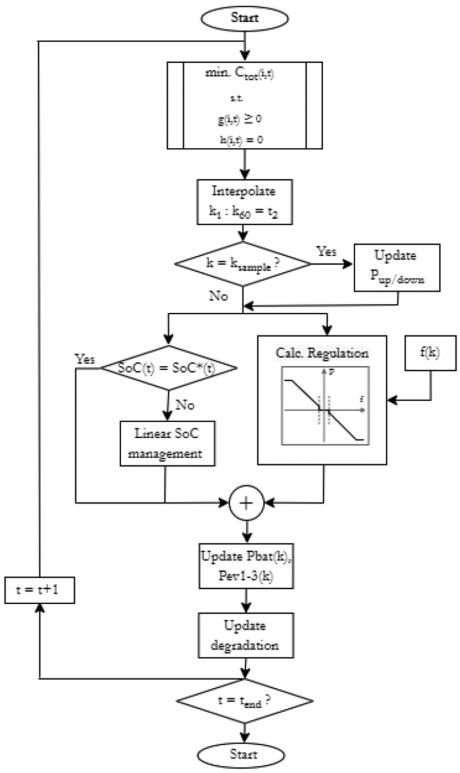

FIG. 13. **Flowchart representing the moving horizon control scheme incorporating optimal scheduling and FCR provision based on droop control.**

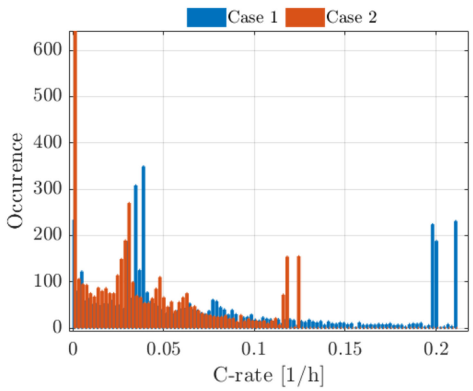

FIG. 14. **Scheduled charging rate occurrence for the case 1-2 BES. The reduced charging rate of the case 2 BES is a reason for the reduced degradation.**

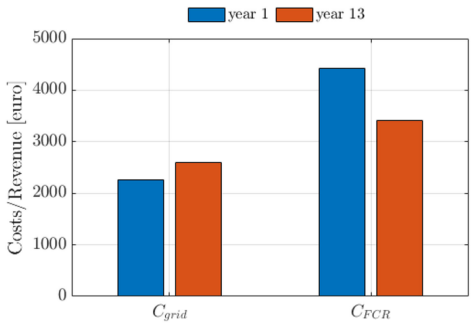

FIG. 15. **Grid energy costs C_{grid} and FCR revenue C_{FCR} of the case 1 model in the first half year, versus the C_{grid} and C_{FCR} in the first half of year 13, just before BES replacement.**

shown in Fig. 15, the regulation revenue decreased by 27.7% an almost one-to-one ratio with the degradation of the battery. Whereas C_{grid} increased by 14.9%. This shows the importance of calculating the degradation of components and the actual costs over their lifetime. Finally, the effect of PV and BES degradation on reserved capacity is shown in Fig. 16. Here the dashed lines indicate the daily average, reserved capacities in the last half-year before BES replacement. The degradation results in an almost one-to-one equivalent decrease of 29% and 14.5% of the reserved power for the BES and PV systems, respectively. Reducing total FCR revenue by 27.7%.

D. SENSITIVITY ANALYSIS

The last part of the results include a sensitivity analysis on the effect of the following input parameters and assumptions.

1) BES price per kWh: V_{BES}^{new}
2) PV system price per kWp: V_{PV}
3) BES Calendar life assumption: c_4
4) Aggregator profit margin: ϵ_{agg}

Fig. 17 shows the result of varying these input parameters on the optimal component sizes. It is concluded that the PV system price does not affect the result, apart from costs.

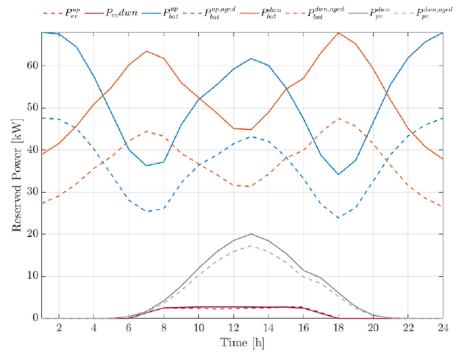

FIG. 16. Average Reserved powers per hour in a day. The striped lines indicate the reserved powers of an aged system.

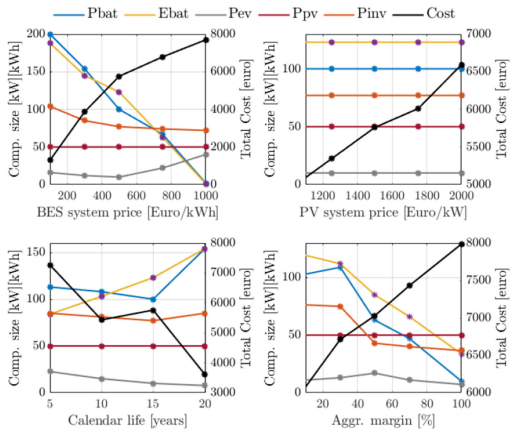

FIG. 17. Sensitivity on input parameters and assumptions.

Furthermore, if the battery prices fall in the future, the BES becomes even more profitable and also higher lifetime revenues can be obtained. Finally, the aggregator profit margin is concluded to be a very important parameter. Up to 30% it does not affect the component sizes much, apart from the revenue. However, for higher profit margins the component ratings decrease, up to the point that they are equal to the values obtained for case 3.

V. CONCLUSION

This paper presents an optimization model which finds the optimal component sizes and power management for an energy management system that integrates a PV system, EV charging, and a BES system. Furthermore, it includes constraints that allow it to reserve power for the FCR market. In its power management, the proposed method combines a unique combination of different business cases, such as energy arbitrage, PV self-consumption, FCR market participation, and second-life BESS value. Based on our results, it is concluded that the highest revenue can be obtained when all aspects are optimally integrated. Additionally, our results indicate that the return on investment for BES systems is still too high for the simulated case without proper control. However, optimal power management adds additional business cases for the BES, such as energy arbitrage and FCR market participation, making the BES very profitable. Finally, by using a moving horizon window control, the significance of PV and BES degradation on total lifetime revenue has been investigated. To summarize, including the FCR market increases lifetime cost-saving by 36% and 460% compared to optimal power management without FCR market participation and nonoptimal power management, respectively, if the second-life value of the BES system is taken into account. Furthermore, our results showed the importance of including component degradation and FCR power provision on lifetime revenue. Investigating the effect of degradation on the reserved powers showed a one-to-one correlation, resulting in a total decrease in FCR market participation of 27.7% at the end of the BES lifetime.

REFERENCES

[1] GOPACS, "The platform to solve congestion in the electricity grid," 2022. Accessed: Apr. 13, 2022. [Online]. Available: https://www.gopacs.eu/

[2] M. Muratori and G. Rizzoni, "Residential demand response: Dynamic energy management and time-varying electricity pricing," *IEEE Trans. Power Syst.*, vol. 31, no. 2, pp. 1108–1117, Mar. 2016.

[3] S. Wang, S. Bi, and Y. A. Zhang, "Demand response management for profit maximizing energy loads in real-time electricity market," *IEEE Trans. Power Syst.*, vol. 33, no. 6, pp. 6387–6396, Nov. 2018.

[4] F. Rassaei, W. Soh, and K.-C. Chua, "Distributed scalable autonomous market-based demand response via residential plug-in electric vehicles in smart grids," *IEEE Trans. Smart Grid*, vol. 9, no. 4, pp. 3281–3290, Jul. 2018.

[5] Q. Yan, B. Zhang, and M. Kezunovic, "Optimized operational cost reduction for an EV charging station integrated with battery energy storage and PV generation," *IEEE Trans. Smart Grid*, vol. 10, no. 2, pp. 2096–2106, Mar. 2019.

[6] V. Pilloni, A. Floris, A. Meloni, and L. Atzori, "Smart home energy management including renewable sources: A QOE-driven approach," *IEEE Trans. Smart Grid*, vol. 9, no. 3, pp. 2006–2018, May 2018.

[7] F. Liberati, A. D. Giorgio, A. Giuseppi, A. Pietrabissa, E. Habib, and L. Martirano, "Joint model predictive control of electric and heating resources in a smart building," *IEEE Trans. Ind. Appl.*, vol. 55, no. 6, pp. 7015–7027, Nov./Dec. 2019.

[8] S. Althaher, P. Mancarella, and J. Mutale, "Automated demand response from home energy management system under dynamic pricing and power and comfort constraints," *IEEE Trans. Smart Grid*, vol. 6, no. 4, pp. 1874–1883, Jul. 2015.

[9] S. Sharma, Y. Xu, A. Verma, and B. K. Panigrahi, "Time-coordinated multienergy management of smart buildings under uncertainties," *IEEE Trans. Ind. Informat.*, vol. 15, no. 8, pp. 4788–4798, Aug. 2019.

[10] A. A. Hadi, C. A. S. Silva, E. Hossain, and R. Challoo, "Algorithm for demand response to maximize the penetration of renewable energy," *IEEE Access*, vol. 8, pp. 55279–55288, 2020.

[11] M. Manganelli, G. Greco, and L. Martirano, "Design of a new architecture and simulation model for building automation toward nearly zero energy buildings," *IEEE Trans. Ind. Appl.*, vol. 55, no. 6, pp. 6999–7007, Nov./Dec. 2019.

[12] F. Hafiz, M. A. Awal, A. R. d. Queiroz, and I. Husain, "Real-time stochastic optimization of energy storage management using deep learning-based forecasts for residential PV applications," *IEEE Trans. Ind. Appl.*, vol. 56, no. 3, pp. 2216–2226, May/Jun. 2020.

[13] X. Tan, G. Qu, B. Sun, N. Li, and D. H. K. Tsang, "Optimal scheduling of battery charging station serving electric vehicles based on battery swapping," *IEEE Trans. Smart Grid*, vol. 10, no. 2, pp. 1372–1384, Mar. 2019.

[14] S.-A. Amamra and J. Marco, "Vehicle-to-grid aggregator to support power grid and reduce electric vehicle charging cost," *IEEE Access*, vol. 7, pp. 178528–178538, 2019.

[15] K. Chaudhari, A. Ukil, K. N. Kumar, U. Manandhar, and S. K. Kollimalla, "Hybrid optimization for economic deployment of ESS in PV-integrated EV charging stations," *IEEE Trans. Ind. Informat.*, vol. 14, no. 1, pp. 106–116, Jan. 2018.

[16] A. Ahmadian, M. Sedghi, B. Mohammadi-ivatloo, A. Elkamel, M. Aliakbar Golkar, and M. Fowler, "Cost-benefit analysis of V2G implementation in distribution networks considering PEVs battery degradation," *IEEE Trans. Sustain. Energy*, vol. 9, no. 2, pp. 961–970, Apr. 2018.

[17] J. Cao, D. Harrold, Z. Fan, T. Morstyn, D. Healey, and K. Li, "Deep reinforcement learning-based energy storage arbitrage with accurate lithium-ion battery degradation model," *IEEE Trans. Smart Grid*, vol. 11, no. 5, pp. 4513–4521, Sep. 2020.

[18] N. Padmanabhan, M. Ahmed, and K. Bhattacharya, "Battery energy storage systems in energy and reserve markets," *IEEE Trans. Power Syst.*, vol. 35, no. 1, pp. 215–226, Jan. 2020.

[19] S. Leonori, G. Rizzoni, F. M. Frattale Mascioli, and A. Rizzi, "Intelligent energy flow management of a nanogrid fast charging station equipped with second life batteries," *Int. J. Elect. Power Energy Syst.*, vol. 127, 2021, Art. no. 106602. [Online]. Available: https://www.sciencedirect.com/science/article/pii/S0142061520313788

[20] Y. Deng, Y. Zhang, F. Luo, and Y. Mu, "Operational planning of centralized charging stations utilizing second-life battery energy storage systems," *IEEE Trans. Sustain. Energy*, vol. 12, no. 1, pp. 387–399, Jan. 2021.

[21] G. R. Chandra Mouli, M. Kefayati, R. Baldick, and P. Bauer, "Integrated PV charging of EV fleet based on energy prices, V2G, and offer of reserves," *IEEE Trans. Smart Grid*, vol. 10, no. 2, pp. 1313–1325, Mar. 2019.

[22] F. Conte, S. Massucco, G.-P. Schiapparelli, and F. Silvestro, "Day-ahead and intra-day planning of integrated bess-PV systems providing frequency regulation," *IEEE Trans. Sustain. Energy*, vol. 11, no. 3, pp. 1797–1806, Jul. 2020.

[23] J. Donadee and M. D. Ilić, "Stochastic optimization of grid to vehicle frequency regulation capacity bids," *IEEE Trans. Smart Grid*, vol. 5, no. 2, pp. 1061–1069, Mar. 2014.

[24] C. Jin, J. Tang, and P. Ghosh, "Optimizing electric vehicle charging with energy storage in the electricity market," *IEEE Trans. Smart Grid*, vol. 4, no. 1, pp. 311–320, Mar. 2013.

[25] E. Yao, V. W. S. Wong, and R. Schober, "Robust frequency regulation capacity scheduling algorithm for electric vehicles," *IEEE Trans. Smart Grid*, vol. 8, no. 2, pp. 984–997, Mar. 2017.

[26] O. Mégel, J. L. Mathieu, and G. Andersson, "Scheduling distributed energy storage units to provide multiple services under forecast error," *Int. J. Elect. Power Energy Syst.*, vol. 72, pp. 48–57, 2015. [Online]. Available: https://www.sciencedirect.com/science/article/pii/S0142061515000939

[27] J. Engels, B. Claessens, and G. Deconinck, "Combined stochastic optimization of frequency control and self-consumption with a battery," *IEEE Trans. Smart Grid*, vol. 10, no. 2, pp. 1971–1981, Mar. 2019.

[28] Y. Shi, B. Xu, D. Wang, and B. Zhang, "Using battery storage for peak shaving and frequency regulation: Joint optimization for superlinear gains," *IEEE Trans. Power Syst.*, vol. 33, no. 3, pp. 2882–2894, May 2018.

[29] B. Cheng and W. B. Powell, "Co-optimizing battery storage for the frequency regulation and energy arbitrage using multi-scale dynamic programming," *IEEE Trans. Smart Grid*, vol. 9, no. 3, pp. 1997–2005, May 2018.

[30] S. Han, S. Han, and K. Sezaki, "Development of an optimal vehicle-to-grid aggregator for frequency regulation," *IEEE Trans. Smart Grid*, vol. 1, no. 1, pp. 65–72, Jun. 2010.

[31] S. Sun, M. Dong, and B. Liang, "Real-time welfare-maximizing regulation allocation in dynamic aggregator-EVs system," *IEEE Trans. Smart Grid*, vol. 5, no. 3, pp. 1397–1409, May 2014.

[32] P. Hasanpor Divshali and C. Evens, "Optimum operation of battery storage system in frequency containment reserves markets," *IEEE Trans. Smart Grid*, vol. 11, no. 6, pp. 4906–4915, Nov. 2020.

[33] A. Oudalov, D. Chartouni, and C. Ohler, "Optimizing a battery energy storage system for primary frequency control," *IEEE Trans. Power Syst.*, vol. 22, no. 3, pp. 1259–1266, Aug. 2007.

[34] S. Kahrobaee, S. Asgarpoor, and W. Qiao, "Optimum sizing of distributed generation and storage capacity in smart households," *IEEE Trans. Smart Grid*, vol. 4, no. 4, pp. 1791–1801, Dec. 2013.

[35] B. Naghibi, M. A. S. Masoum, and S. Deilami, "Effects of V2H integration on optimal sizing of renewable resources in smart home based on monte carlo simulations," *IEEE Power Energy Technol. Syst. J.*, vol. 5, no. 3, pp. 73–84, Sep. 2018.

[36] S. Bandyopadhyay, G. R. Chandra Mouli, Z. Qin, L. R. Elizondo, and P. Bauer, "Techno-economical model based optimal sizing of PV-battery systems for microgrids," *IEEE Trans. Sustain. Energy*, vol. 11, no. 3, pp. 1657–1668, Jul. 2020.

[37] Y. Yang, H. Li, A. Aichhorn, J. Zheng, and M. Greenleaf, "Sizing strategy of distributed battery storage system with high penetration of photovoltaic for voltage regulation and peak load shaving," *IEEE Trans. Smart Grid*, vol. 5, no. 2, pp. 982–991, Mar. 2014.

[38] T. M. Masaud and E. F. El-Saadany, "Correlating optimal size, cycle life estimation, and technology selection of batteries: A two-stage approach for microgrid applications," *IEEE Trans. Sustain. Energy*, vol. 11, no. 3, pp. 1257–1267, Jul. 2020.

[39] F. Hafiz, A. R. de Queiroz, P. Fajri, and I. Husain, "Energy management and optimal storage sizing for a shared community: A multi-stage stochastic programming approach," *Appl. Energy*, vol. 236, pp. 42–54, 2019.

[40] J. von Appen and M. Braun, "Sizing and improved grid integration of residential PV systems with heat pumps and battery storage systems," *IEEE Trans. Energy Convers.*, vol. 34, no. 1, pp. 562–571, Mar. 2019.

[41] R. Atia and N. Yamada, "Sizing and analysis of renewable energy and battery systems in residential microgrids," *IEEE Trans. Smart Grid*, vol. 7, no. 3, pp. 1204–1213, May 2016.

[42] A. Saez-de Ibarra, E. Martinez-Laserna, D.-I. Stroe, M. Swierczynski, and P. Rodriguez, "Sizing study of second life li-ion batteries for enhancing renewable energy grid integration," *IEEE Trans. Ind. Appl.*, vol. 52, no. 6, pp. 4999–5008, Nov./Dec. 2016.

[43] G. Graber, V. Galdi, V. Calderaro, and P. Mancarella, "A stochastic approach to size ev charging stations with support of second life battery storage systems," in *Proc. IEEE Manchester PowerTech*, 2017, pp. 1–6.

[44] S. Paul and N. P. Padhy, "Real-time bilevel energy management of smart residential apartment building," *IEEE Trans. Ind. Informat.*, vol. 16, no. 6, pp. 3708–3720, Jun. 2020.

[45] R. Fu, T. Remo, and R. Margolis, "U.S. utility-scale photovoltaics plus-energy storage system costs benchmark," Dec. 2015. Accessed: Apr. 13, 2022. [Online]. Available: https://www.nrel.gov/docs/fy19osti/71714.pdf

[46] A. Singh, S. Reese, and S. Akar, "Performance and techno-economic evaluation of a three-phase, 50-kW SiC-based PV inverter," in *Proc. IEEE 46th Photovolt. Specialists Conf.*, 2019, pp. 0695–0701.

[47] K. Kelly, K. Smith, J. Cosgrove, B. Prohaska, and A. Pesaran, "Battery ownership model - medium duty HEV battery leasing & standardization," Nat. Renewable Energy Lab., Tech. Rep., 2015. [Online]. Available: https://www.nrel.gov/docs/fy16osti/66140.pdf

[48] TenneT TSO b.v., "Battery storage in the United States: An update on market trends," Energy Inf. Agency, Tech. Rep., Netherlands, 28 Jun. 2018. Accessed: Apr. 13, 2022. [Online]. Available: https://www.tennet.eu/fileadmin/user_upload/SO_NL/FCR_Final_report_FCR_pilot__alleen_in_Engels_.pdf

[49] I. Mathews, B. Xu, W. He, V. Barreto, T. Buonassisi, and I. M. Peters, "Technoeconomic model of second-life batteries for utility-scale solar considering calendar and cycle aging," *Appl. Energy*, vol. 269, 2020, Art. no. 115127. [Online]. Available: https://www.sciencedirect.com/science/article/pii/S0306261920306395

[50] TenneT, "Final report FCR pilot," *TenneT Holding BV*, The Netherlands, 2018.

[51] TenneT TSO b.v., "FCR manual for BSP's, holding BV, The Netherlands," Tech. Rep., 2022. Accessed: Apr. 13, 2022. [Online]. Available: https://www.tennet.eu/fileadmin/user_upload/SO_NL/Handboek_FCR_voor_BSPs_-_EN_version.pdf

[52] ENTSOE, "Price of reserved balancing reserves," ENTSOE, 2019, Accessed: Apr. 4, 2022. [Online]. Available: https://transparency.entsoe.eu/balancing/r2/balancingVolumesReservationPrice/show

[53] G. R. Chandra Mouli, J. H. Schijffelen, P. Bauer, and M. Zeman, "Design and comparison of a 10-kW interleaved boost converter for PV application using SI and SIC devices," *IEEE Trans. Emerg. Sel. Topics Power Electron.*, vol. 5, no. 2, pp. 610–623, Jun. 2017.

[54] J. S. Stein, C. Robinson, B. King, C. Deline, S. Rummel, and B. Sekulic, "PV lifetime project: Measuring PV module performance degradation: 2018 indoor flash testing results," in *Proc. IEEE 7th World Conf. Photovolt. Energy Convers. (WCPEC)*, 2108, pp. 0771–0777, doi: 10.1109/PVSC.2018.8547397.

[55] Europe-SolarStore.com, "LG chem resu 10 H - 400V lithium-ion storage battery," Accessed: Apr. 13, 2022. [Online]. Available: https://www.europe-solarstore.com/lg-chem-resu-10h-400v-lithium-ion-storage-battery.html
[56] S. Käbitz *et al.*, "Cycle and calendar life study of a $|LiNi_1/3Mn_1/3Co_1/3O_2$ (NMC) li-ion high energy system. Part A: Full cell characterization," *J. Power Sources*, vol. 239, pp. 572–583, 2013. [Online]. Available: https://www.sciencedirect.com/science/article/pii/S0378775313004369
[57] I. Baghdadi, O. Briat, J.-Y. Delétage, P. Gyan, and J.-M. Vinassa, "Lithium battery aging model based on dakin's degradation approach," *J. Power Sources*, vol. 325, pp. 273–285, 2016. [Online]. Available: https://www.sciencedirect.com/science/article/pii/S0378775316307388
[58] D. van der Meer, G. R. Chandra Mouli, G. Morales-España Mouli, L. R. Elizondo, and P. Bauer, "Energy management system with PV power forecast to optimally charge EVs at the workplace," *IEEE Trans. Ind. Informat.*, vol. 14, no. 1, pp. 311–320, Jan. 2018.
[59] J. Wang *et al.*, "Degradation of lithium ion batteries employing graphite negatives and nickel-cobalt-manganese oxide spinel manganese oxide positives: Part 1, aging mechanisms and life estimation," *J. Power Sources*, vol. 269, pp. 937–948, 2014. [Online]. Available: https://www.sciencedirect.com/science/article/pii/S037877531401074X
[60] I. Baccouche, S. Jemmali, B. Manai, N. Omar, and N. E. B. Amara, "Improved OCV model of a li-ion NMC battery for online SOC estimation using the extended Kalman filter," *Energies*, vol. 10, May 2017, Art. no. 764.
[61] H. Yoshida, N. Imamura, T. Inoue, K. Takeda, and H. Naito, "Verification of life estimation model for space lithium-ion cells," *Electrochemistry*, vol. 78, no. 5, pp. 482–488, 2010.
[62] N. Voulis, "Harnessing heterogeneity understanding urban demand to support the energy transition," Ph.D. dissertation, Delft Univ. Technol., Delft, CD, Netherlands, 2019. Accessed: Apr. 13, 2022. [Online]. Available: https://research.tudelft.nl/en/publications/harnessing-heterogeneity-understanding-urban-demand-to-support-th
[63] N. Sadeghianpourhamami, N. Refa, M. Strobbe, and C. Develder, "Quantitive analysis of electric vehicle flexibility: A data-driven approach," *Int. J. Elect. Power Energy Syst.*, vol. 95, pp. 451–462, 2018.
[64] J. Helmus, J. Spoelstra, N. Refa, M. Lees, and R. van den Hoed, "Assessment of public charging infrastructure push and pull Rollout strategies: The case of The Netherlands," *Energy Policy*, vol. 121, pp. 35–47, 2018.
[65] KNMI, "Forecast of solar radiation in The Netherlands," 2019. Accessed: Apr. 13, 2022. [Online]. Available: https://www.knmi.nl/research/observations-data-technology/projects
[66] N. R. E. Laboratory, "Cost-reduction roadmap for residential solar photovoltaics (PV), 2017–2030," 2018. Accessed: Apr. 13, 2022. [Online]. Available: https://www.nrel.gov/docs/fy18osti/70748.pdf
[67] C. Nelder and E. Rogers, "Reducing EV charger infrastructure costs," Rocky Mountain Inst., Tech. Rep., US, 2019. Accessed: Apr. 13, 2022. [Online]. Available: https://rmi.org/ev-charging-costs

WILJAN VERMEER (Student Member, IEEE) received the bachelor's degree in electrical engineering from the Eindhoven University of Technology, Eindhoven, The Netherlands, in 2016, and the master's degree in electrical engineering in 2018 from the Delft University of Technology, Delft, The Netherlands, where he has been working toward the Ph.D. degree in the field of solar-powered smart charging systemssince 2018. His research interests include EV smart charging, battery degradation, and DC-DC power electronic converters for smart charging.

GAUTHAM RAM CHANDRA MOULI (Member, IEEE) received the bachelor's degree in electrical engineering from the National Institute of Technology Trichy, Trichy, India, in 2011, the master's degree in electrical engineering from the Delft University of Technology (TU Delft), Delft, The Netherlands, in 2013, and the Ph.D. degree from TU Delft, in 2018, for the development of a solar powered V2G electric vehicle charger compatible with CHAdeMO, CCS/COMBO and designed smart charging algorithms (with PRE, ABB, and UT Austin). He is currently an Assistant Professor with the DC systems, Energy conversion and Storage Group, Department of Electrical Sustainable Energy, Delft University of Technology. From 2017 to 2019, he was a Postdoctoral Researcher with TU Delft pursuing his research on power converters for EV charging, smart charging of EVs, trolley busses. He is involved in many projects with industrial and academic partners at national and EU level concerning electric mobility and renewable energy, such as PV charging of electric vehicles, OSCD, Trolley 2.0, Flexgrid, Flexinet, and NEON. He is the Coordinator and a Lecturer for Massive Open Online Course (MOOC) on Electric cars on edX.org with 175,000 learners from 175 countries. He is also the Vice-Chair of IEEE Industrial Electronic Society Benelux chapter. His current research research interests include electric vehicles & charging, PV systems, power electronics, and intelligent control. He was awarded the most significant innovation in electric vehicles award from IDtechEx in 2018 and Best Tech Idea of 2018 by KIJK.

He was also awarded the Best Paper prize in the IEEE TRANSACTIONS ON INDUSTRIAL INFORMATICS in 2018, Best Poster prize at Erasmus Energy Forum 2016, Netherlands, and Best Paper prize at the IEEE INDICON Conference 2009, India.

PAVOL BAUER (Senior Member, IEEE) received the master's degree in electrical engineering from the Technical University of Kosice, Košice, Slovakia, in 1985, and the Ph.D. degree from the Delft University of Technology, Delft, The Netherlands, in 1995. He is currently a Full Professor with the Department of Electrical Sustainable Energy, Delft University of Technology, the Head of DC Systems, Energy Conversion and Storage Group, a Professor with the Brno University of Technology, Brno, Czechia, and a Honorary Professor with Politehnica University Timişoara, Timişoara, Romania. From 2002 to 2003, he was with KEMA (DNV GL, Arnhem) on different projects related to power electronics applications in power systems. He has worked on many projects for industry concerning wind and wave energy, power electronic applications for power systems, such as Smarttrafo, HVDC systems, projects for smart cities such as PV charging of electric vehicles, PV and storage integration, contactless charging, and participated in several Leonardo da Vinci, H2020 and Electric Mobility Europe EU projects as a Project Partner (ELINA, INETELE, E-Pragmatic, Micact, Trolley 2.0, OSCD, P2P, Progressus) and a Coordinator (PEMCWebLab.com-Edipe, SustEner, Eranet DCMICRO). He has authored or coauthored more than 120 journal and 500 conference papers, in his field with H factor Google scholar 40, Web of Science 26, he is the author or coauthor of eight books, holds seven international patents and organized several tutorials at the international conferences. His main research interests include power electronics for charging of electric vehicles and dc grids. He is the former Chairman of Benelux IEEE Joint Industry Applications Society, Power Electronics and Power Engineering Society chapter, the Chairman of the Power Electronics and Motion Control council, Member of the Executive Committee of European Power Electronics Association and International Steering Committee at numerous conferences.